Proceedings of ASME Turbo Expo 2003
Power for Land, Sea, and Air
June 16-19, 2003, Atlanta, Georgia, USA

GT2003-38939

OPTIMIZING THE VANE-ENDWALL JUNCTION TO REDUCE ADIABATIC WALL TEMPERATURES IN A TURBINE VANE PASSAGE

Andrew T. Lethander and Karen A. Thole
Mechanical Engineering Department
Virginia Polytechnic Institute and State University
Blacksburg, VA 24060

Gary Zess and Joel Wagner
Pratt & Whitney
400 Main Street
East Hartford, CT 06108

ABSTRACT

Secondary flows in airfoil passages have become increasingly important in the design of modern gas turbines due to several fundamental trends in gas turbine engine development. Driven to achieve higher engine efficiencies and specific thrust output, the gas turbine industry is continually pushing the envelope of maximum allowable turbine inlet temperature. While many researchers have worked to gain an understanding of secondary flows and their effects on turbine heat transfer, very few have pursued ways to passively mitigate their detrimental effects.

While considerable attention has been given to techniques of secondary flow reduction in order to minimize the associated aerodynamic losses, the objective of this study was to improve the thermal environment for a turbine vane. In particular, this objective was achieved through optimizing a fillet in the vane-endwall juncture to minimize adiabatic wall temperatures. The approach taken was to employ a commercial optimization software package in conjunction with a computational fluid dynamics (CFD) package in the design of the fillet. Results indicate that a significant reduction in adiabatic wall temperatures can be achieved through application of an optimized fillet.

INTRODUCTION

Secondary flows, which have become extremely important in the design of modern gas turbines, refers to the vortical structures that develop in airfoil passages. This development is a result of strong turning and non-uniform flow conditions at the inlet. Both the losses in total pressure and the distortion of the thermal field through a turbine are attributed to secondary flow effects. While the development of the vortical structures originates in the endwall regions, the growth can be such that at the exit a large portion of an airfoil passage is affected.

A simple argument can be used to describe the origin of secondary flows in turbine passages. Consider two different streamlines passing through a nozzle guide vane, one originating in the inviscid freestream and the other in the platform boundary layer. With the same circumferential pressure gradient imposed on both streamlines and knowing that this pressure gradient must be balanced by the centripetal acceleration, the two radii of curvature of the streamlines must be different. The curvature of the streamline originating in the boundary layer will be smaller than that of the streamline in the inviscid region. The deviation in flow path between these streamlines results in the development of the secondary flows.

Many of the past studies on secondary flow effects have focused on the aerodynamic penalties resulting in total pressure losses through a stage. Arguably as important, however, are the thermal penalties resulting in reduced airfoil life. This is particularly true since increased turbine inlet temperatures are desired to achieve high thrust-to-weight ratios for aero engines. While vanes and blades are cooled with compressor bleed air, the platform regions provide a particularly difficult challenge because of the secondary flows present and because of the additional aerodynamic penalties introduced by the cooling air.

Unlike the majority of past studies, the primary focus of the research effort presented in this paper is to reduce the severity of the thermal environment that the first vane must endure. The approach to improving the thermal environment is to provide a fillet structure in the vane-platform juncture. In particular, optimization studies were performed to design a fillet in which the objective function was to minimize the adiabatic temperatures of the vane and its associated platform (endwall). The work discussed in this paper presents the first optimization study presented in the open literature in which reducing the adiabatic wall temperatures were imposed as the objective. In addition, this study is unique because it is the first reported attempt in which two commercial software packages, FLUENT and iSIGHT, were mated to perform this optimization. While FLUENT was used as the flow solver, iSIGHT was used to perform the optimization algorithms.

Following a review of the past literature, the optimization process and results from the optimization studies will be presented. Comparisons will then be made for the predicted flow and thermal fields for a vane having a manufacturing fillet (baseline) and an optimized fillet.

PREVIOUS STUDIES

Methods for reducing the secondary flows in turbine passages have ranged from simple fillet designs for two-dimensional airfoils to full three-dimensional endwall contour designs on three-dimensional airfoils. The aim of most past studies, as mentioned previously, has been to reduce the aerodynamic losses and flow angle deviations at the passage exit. The open literature shows conflicting results in that some studies indicate an overall definitive reduction in losses while other studies have shown overall increases in loss even though a local reduction in loss was concentrated near the unprofiled endwall. More recently, however, there have been a series of papers on endwall contouring indicating an overall reduction in losses and secondary flows using a methodical approach involving computational fluid dynamics followed by experimental validation.

Three-dimensional endwall contouring was investigated computationally by Harvey, et al. [1] and experimentally verified by Hartland, et al. [2]. To design the endwall contour, they used a linear sensitivity matrix in conjunction with superposition methods prior to applying an inverse design algorithm. Mathematically, perturbations to the cosine and sine functions that described the fillet were made to ultimately arrive at an optimum configuration. The results of the experimental verification confirmed a predicted reduction in exit flow angle deviations. Moreover, the experiments indicated a 30% reduction in loss, which was higher than predicted. One plausible reason for a disagreement between the experiments and computations may be the fact that the turbulence levels (and/or unsteady vortex movement) were not accurately predicted with two-equation models. Turbulence is a large contributor to secondary losses (Gregory-Smith and Cleak [3]). In a later study, Brennan, et al. [4] and Rose, et al. [5] applied similar computational and experimental (respectively) methodologies as Harvey et al. [1] and Hartland, et al. [2]. They applied these methods to a high pressure turbine for a single stage in both the vane and blade passages. They reported stage efficiency improvements of 0.59%, which exceeded their predicted improvement of 0.4%.

Sauer, et al. [6] investigated the application of a leading edge "bulb" for secondary flow loss reduction. The objective of the leading edge bulb was to increase the strength of the suction side leg of the horseshoe vortex thereby affecting the passage vortex strength and its interaction with the airfoil boundary layers. For the best bulb design, Sauer et al. measured a 50% reduction in total pressure loss. Computational fluid dynamics results qualitatively agreed with their experimental measurements; however, no flow field measurements within the blade passage were presented for comparison.

While these previous studies have made detailed total pressure traverses and the work of Rose, et al. [5] included hot-wire traverses, Zess and Thole [7] fully-resolved mean and turbulent flow measurements for a juncture fillet they applied to a large-scale model of a nozzle guide vane. They designed their fillet using the same CFD package as that reported in this paper with the goal of mitigating the formation of the horseshoe vortex. The fillet that they designed accelerated the boundary layer thereby flattening the total pressure profile at the vane leading edge preventing development of the horseshoe vortex. Although several different fillet shapes and sizes were investigated using CFD, ultimately a straight fillet that was one boundary layer thickness in height and extended two boundary layer thicknesses axially upstream was predicted to be successful. Upon completion of the fillet design, flow field measurements verified the performance of the leading edge fillet with no horseshoe vortex being present. Although the passage vortex did develop for the filleted vane, it was not as well developed as for the unfilleted vane. Good agreement between computational and experimental results was observed not only at the leading edge but also within the passage.

The only paper to have considered the endwall heat transfer effects has been that of Shih and Lin [8] who performed a computational study to evaluate two different fillet designs with and without inlet swirl. Their study indicated a reduction of heat transfer by more than 10% on the airfoil and by more than 30% on the endwall.

Using endwall contouring and leading edge fillets show promise in reducing secondary flow losses; however, the potential impact of these technologies on endwall cooling from the combustor liner has not yet been considered. In this investigation, the shape of a juncture fillet will be optimized with the goal of minimizing adiabatic wall temperatures, which is one important aspect in reducing the overall endwall heat transfer. The differences between this study and that previously reported by Shih and Lin [8] are that we are aiming at using combustor coolant for the endwall and are considering realistic combustor exit profiles.

PROBLEM APPROACH

There are no known integrated commercial CFD/optimization packages and as such a significant effort in designing the fillet was devoted to this integration. The computational fluid dynamics (CFD) package chosen for this study is a product of Fluent, Inc. called Fluent [9]. The primary reason for selecting FLUENT was because of the previous benchmark studies in which the secondary flow field was correctly predicted for both unfilleted (Hermanson and Thole, 1999) and filleted (Zess and Thole [7]) vanes. In addition, GAMBIT [10] (the mesh generator) has the ability to grid complex geometries using unstructured meshing techniques. The optimization software is a product of Engineous Software, Inc. and is called iSIGHT (Engineous Software, Inc. [11]). iSIGHT is best described as a shell that provides a number of different optimization algorithms.

Computational Fluid Dynamics Simulations

Second order accuracy was used in solving the Reynolds-averaged Navier-Stokes equations, energy equation, and turbulence model equations. Turbulence was modeled using the RNG k-ε model (Yakhot, et al. [12]) with non-equilibrium wall functions to model the near-wall region (Kim and Choudhury [13]). These turbulence models were applied because it was previously found that reasonably good predictions were made as compared with measured secondary

velocities while still maintaining computational efficiency (Zess and Thole [7]).

An illustration of the computational domain with a fillet is shown in Figure 1. The turbine vane geometry used in this research is from an advanced, commercial turbine and has been reported in the past by Radomsky and Thole [14, 15, and 16] and Zess and Thole [7]. For the purpose of wind tunnel testing in a later study, the scaled-up vane geometry (9X) was used for the computations while maintaining matched Reynolds number conditions ($Re_{in} = 2.3x10^5$). The vane is two-dimensional whereby the geometry is that of the commercial vane's midspan. For consistency with future experiments, a linear cascade was modeled with an inlet velocity of 6.3 m/s (Ma = 0.02). Because of the large-scale experiment, the Mach number was not matched, but the Reynolds number was matched.

The inlet of the domain was located one chord upstream of the vane stagnation location, which was far enough upstream to eliminate the influence of the vane on the inlet conditions. The exit of the domain is located 1.5 chords from the vane trailing edge in the exit flow direction of 78 degrees. To prevent highly skewed cells, an additional 0.1 chord was added in the axial direction. Periodicity boundary conditions were placed on the side faces of the computational domain while a symmetry boundary condition was applied at mid-span. Adiabatic boundary conditions were applied to the endwall, fillet, and vane surfaces.

The mesh that was used was unstructured with typical sizes being $9x10^5$ cells. The mesh that was used was arrived upon through previous grid sensitivity studies using the adaption capabilities of FLUENT. In assessing the grid sensitivity for the final fillet design, grid adaptions were completed using y^+ values and temperature gradients. The adaptions using y^+ values resulted in a grid size that was $1.2x10^6$ cells. The larger grid gave a maximum difference in effectiveness, which occurred on the suction side of the airfoil, of less than $\Delta\eta = 0.005$. Adaptions using temperature gradients resulted in no detectable change in effectiveness. When computing the overall decrease in wall temperatures the change in the percentage improvement, where this percentage is defined by equation (4), was at most 0.27% between the two different meshes. The RANS, energy, and turbulence equations were computed until the residual values of the computations converged. The convergence of residuals for continuity, *x*-momentum, *y*-momentum, *z*-momentum, *k* and ε were resolved to levels of 10^{-4} with the exception of the energy equation

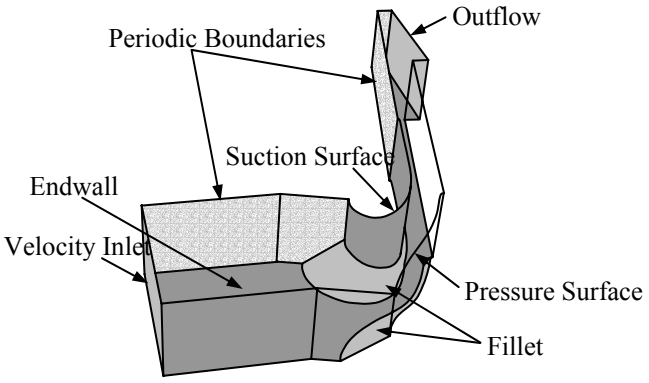

Figure 1. Computational domain for CFD simulations.

which was set to a level of 10^{-6}. Computations required 700 iterations for this convergence criteria. This Increasing the number of iterations by 10% resulted in a negligible change in effectiveness levels.

The inlet boundary conditions for a preliminary optimization test case were adapted from previous work reported by Hermanson and Thole [17] and are shown in Figure 2. All boundary conditions were assumed to be uniform in the pitchwise (circumferential) direction. A two-dimensional boundary layer code called TEXSTAN (Crawford [18]) was used to generate spanwise (radial) profiles of velocity, turbulent kinetic energy, and turbulence dissipation rate for the inlet boundary layer. The velocity boundary layer thickness was 9.1 % of the total vane span. Based on a turbulent boundary layer profile and the temperature profile shown in Figure 2b, the resulting total pressure profile approaching the vane is shown in Figure 2c. The approaching total pressure profile peaks at nominally 10% of the span. This profile results in a secondary flow field in which there is a split at this location with flow being driven towards the platform and towards the midspan from this location, as will be shown in the results section of this paper.

Integration of Optimization Shell and CFD Package

Prior to discussing the specifics of the integration of iSIGHT and Fluent, it is instructive to consider how iSIGHT works in a generic sense. As an optimization shell, iSIGHT is designed to run simulation codes that are executed from a command line and use structured text files as input and output. Through iSIGHT's file parsing capability, the results of a simulation can be retrieved from the output file(s) and evaluated. Based on the results, iSIGHT then modifies the design parameters in the input file and continues to execute the simulation code. This process continues until iSIGHT converges on an optimum design. Guided by the problem definition and optimization routine, iSIGHT automates simulation code execution, data retrieval, and iterative adjustment of the design parameters. In the optimization effort reported in this paper an exploratory optimization technique, called simulated annealing, was employed. Simulated annealing is considered an exploratory technique because it avoids focusing only on a local region of the design space. In this way, simulated annealing provides fairly good coverage of the design space in its search for a global optimum.

To link iSIGHT with the Fluent CFD package, extensive use was made of the journaling features of Fluent and the Fluent preprocessor, Gambit. Journaling allows for the creation of so-called journal files that can subsequently be specified as input to the simulation code and executed from the command line. A journal file is a simple text file that contains a sequential set of program commands that are to be executed. Thus, the journal files for Gambit and Fluent serve as the simulation code input files. Using the file parsing capabilities of iSIGHT, design parameters specified in these files can be automatically altered between design iterations.

Since the goal is to optimize fillet shape, the solution domain was altered between CFD runs. This was achieved by creating a parametric model of the turbine vane leading edge fillet and applying the model to geometry creation within the Gambit journal file. Fortunately, the journaling capabilities of

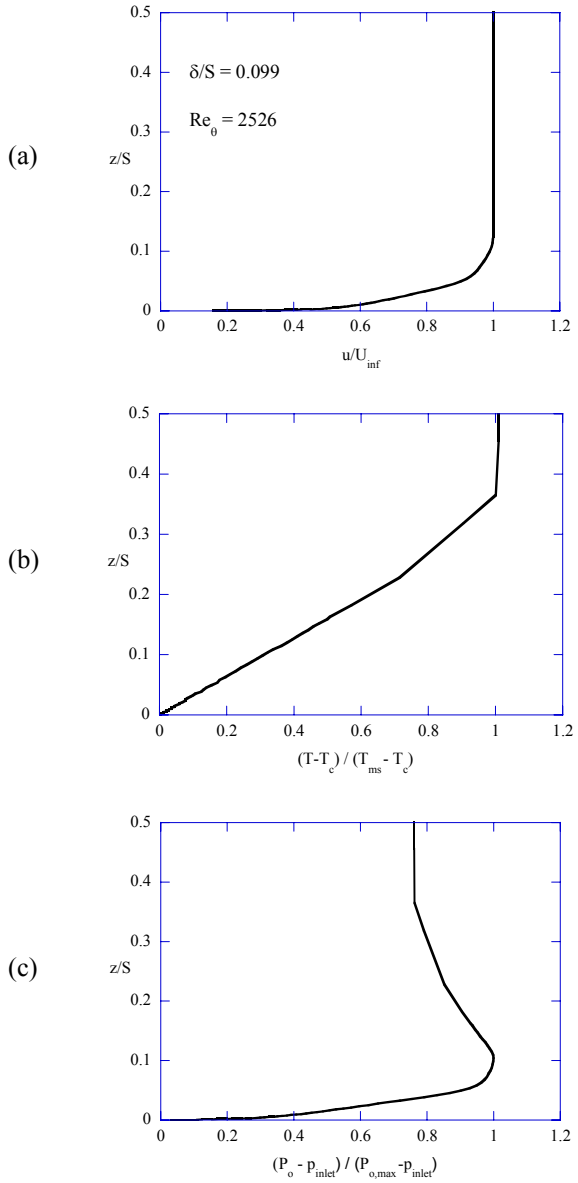

Figure 2a-c. Inlet radially-varying boundary conditions of (a) velocity, (b) temperature, and (c) total pressure.

Gambit allowed for the specification of parameters and the use of parameters in mathematical expressions. By specifying these geometric parameters to be design variables, iSIGHT has the ability to alter the shape of the fillet between simulation runs.

To minimize the number of design parameters for the leading edge fillet, a mathematical model of the fillet was developed. The leading edge fillet geometry and associated design parameters are illustrated in Figure 3. A total of four design parameters were selected to describe the shape of a fillet. These parameters included the maximum fillet height, H_{max}, the maximum fillet extent normal to the vane surface, D_{max}, and the extensions of the fillet along the vane pressure and suction surfaces, $s_{max,ps}$ and $s_{max,ss}$. One of the restrictions of this parametric description was that the maximum height and extent of the fillet were fixed at the vane dynamic stagnation. For simplicity, a linear profile in the span direction was used. In addition to the leading edge fillet, a standard manufacturing fillet was included in the computational model beyond the $s_{max,ps}$ and $s_{max,ss}$ locations of the vane.

The constraints applied to the fillet in this investigation were the following:

$$\begin{aligned} 0.084 &\le D_{max}/C \le 0.227 \\ 0.042 &\le H_{\max}/C \le 0.227 \\ 0.100 &\le s_{\max,ps}/s_{total,ps} \le 0.970 \\ 0.085 &\le s_{\max,ss}/s_{total,ss} \le 0.440 \end{aligned} \quad (1)$$

These constraints insured that the gage point remained the same and also insured that the fillet size did not become impractical from a manufacturing standpoint.

Objective Function Definition and Evaluation

The goal of this investigation was to minimize the surface temperatures experienced by the endwall and vane. Since these surfaces were modeled as adiabatic, definition of an objective function appeared to be straightforward. At the start of this optimization effort, the area-weighted average surface temperature of the vane, endwall, and fillet were selected as the objective function. However, this objective function did not take into account possible local hot spots, which can be quite important in considering airfoil life. As such, minimizing the area-weighted average of the square of the surface temperature was used indicated below:

$$F(\mathbf{X}) = \frac{1}{A}\iint_A T_{aw}^2 dA \quad (2)$$

The **X** vector in equation 2 represents the design variables that were considered for this study. Note that the area considered included the vane, platform, and fillet surface area. The area on the endwall that was considered extended from 50.6% of the axial chord upstream of the vane stagnation to 10% of the axial chord downstream of the vane trailing edge.

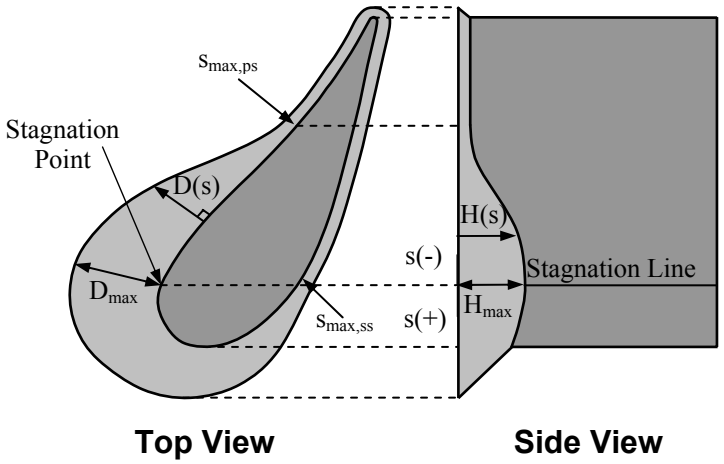

Figure 3. Leading-edge fillet and associated geometric design parameters.

OPTIMIZATION RESULTS

Through analysis of the optimization results, the relative importance of four different design variables was determined. During the optimization process, iSIGHT maintained a database of all 64 simulations that were performed, recording the design variables and the resulting value of the objective function for each. For comparison purposes, a baseline simulation was performed that only contained the manufacturing fillet (actual engine fillet radius of 1.3 mm). Although the baseline geometry includes a standard manufacturing fillet, no notable effect of this fillet on the secondary flows were noted as compared to a vane with a sharp 90° juncture. The objective function (equation 2) was normalized by the calculated value for the vane with a manufacturing fillet for determining the performance relative to the vane having no fillet.

$$F_{norm}(\mathbf{X}) = \frac{\frac{1}{A}\iint_A T_{aw}^2 dA}{\left.\frac{1}{A}\iint_A T_{aw}^2 dA\right|_{Baseline}} \qquad (3)$$

The normalized objectives for each design variable are shown in Figures 4a-d. From these plots, a general indication for the dependence of the objective on each design variable can be obtained. Note that all of the plots indicate $F_{norm} < 1$, which means that all of the cases indicate improved thermal performance of the vane. The plot that appears to show the most definitive trend is that of the objective versus the maximum fillet height (Figure 4a). This plot clearly illustrates a reduction of the objective, the desired result, as the maximum fillet height increases. Figure 4b shows the next highest correlation of improved thermal benefit with the fillet geometry being the maximum extent. Improved performance as a function of the fillet length around the suction side showed very little correlation. Although it is not shown here, similar results (very little correlation) occur as a function of fillet length around the pressure surface. Figure 4d shows the normalized objective function plotted against the combined suction and pressure side wrap around distances. The combined distances showed a somewhat better correlation with improved performance than each of the distances alone.

Given that H_{max} and D_{max} provided the strongest correlation with that of the objective function, a contour plot of the objective was constructed over the design space that was considered as shown in Figure 5. This plot clearly indicates that designs with large values of these two variables yielded the best fillet performance. Figure 5 indicates that improved performance can be achieved with the largest fillets that were considered in this study. Although the design space considered appears to be too confining, applying fillets larger than this size may be impractical due to the interference with the upstream combustor.

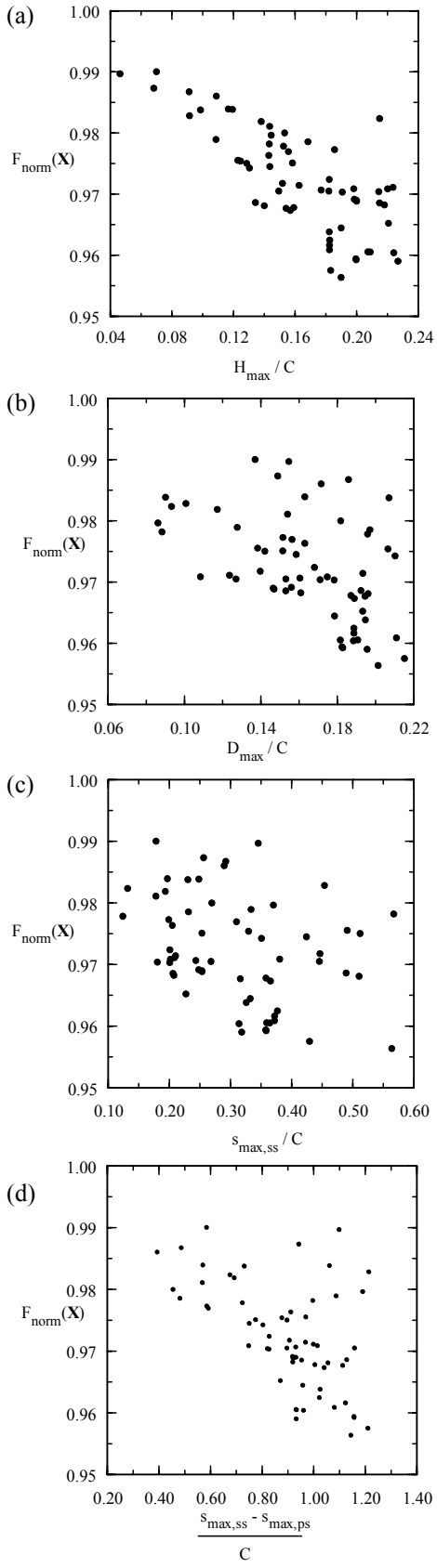

Figure 4a-d. Thermal benefit as affected by (a)maximum fillet height, (b)maximum fillet extent, (c)extent along suction surface, and (d)combined extent along suction and pressure surfaces.

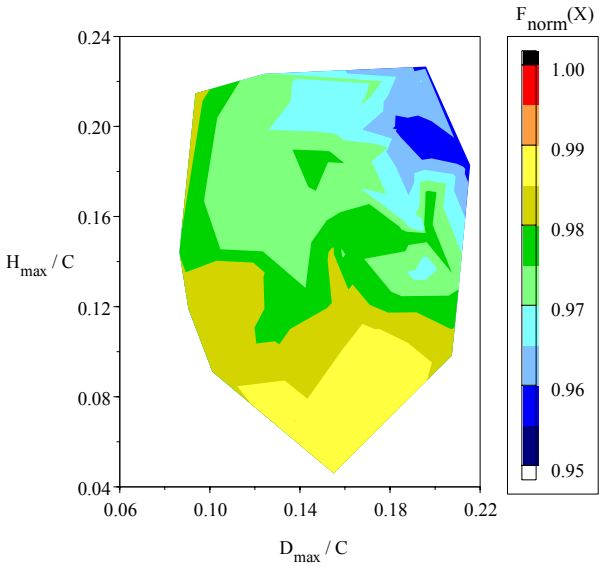

Figure 5. Contours of thermal benefit as affected by maximum fillet height and extent normal to the vane.

Comparison of Baseline and Optimized Fillet Cases

Comparisons of the optimized fillet case to that of the baseline were made to understand why an improved thermal performance was achieved and to determine the effects that the fillet had on the aerodynamic performance. The final fillet design had the geometric characteristics listed in Table 1. As noted from Table 1, the linear fillet chosen was very large as dictated by the optimization study.

Table 1. Summary of Optimized Fillet Geometry

Feature	Fillet Size
H_{max}/C	0.20
D_{max}/C	0.20
$S_{max,ss}/C$	0.56
$S_{max,ps}/C$	-0.58

The static pressure distribution for the baseline and filleted vanes at the vane midspan are shown in Figure 6. The static pressure at the mid-span is predicted to be slightly affected by the fillet over a small portion of the suction surface. Along the suction surface, the lower Cp values are a result of the increased acceleration due to the fillet. There was a 1.6% increase in total pressure loss predicted for the filleted vane relative to the baseline. This percentage increase is based on the difference between mass-averaged total pressure difference between the inlet and outlet of the filleted vane to that of the baseline case all normalized by the baseline case. Although there was an increase, it is relatively small considering that this percentage is normalized by that of the baseline vane's total pressure loss.

Streamlines released upstream of the vane for both the baseline and filleted vanes are shown in Figures 7a-b. The color of the streamlines represents the magnitude of the spanwise velocity component (w) normalized by the mainstream. The streamline pattern indicates the general turning pattern for the baseline showing the development of thepassage vortex. For the optimized fillet case, however, the streamline pattern indicates that the flow is following the

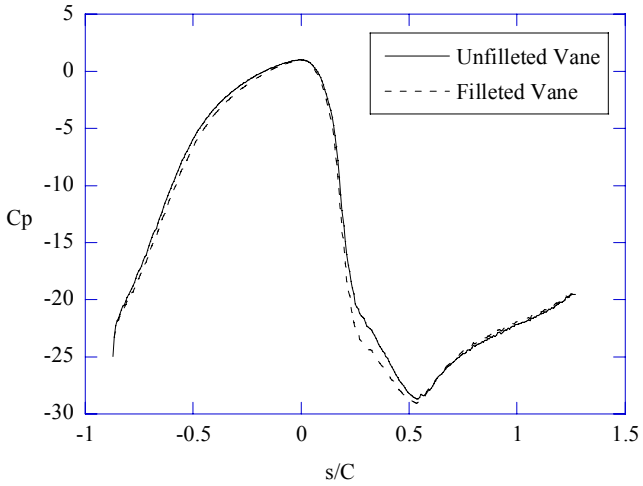

Figure 6. Comparison of the predicted pressure distributions for the baseline unfilleted vane and optimum filleted vane.

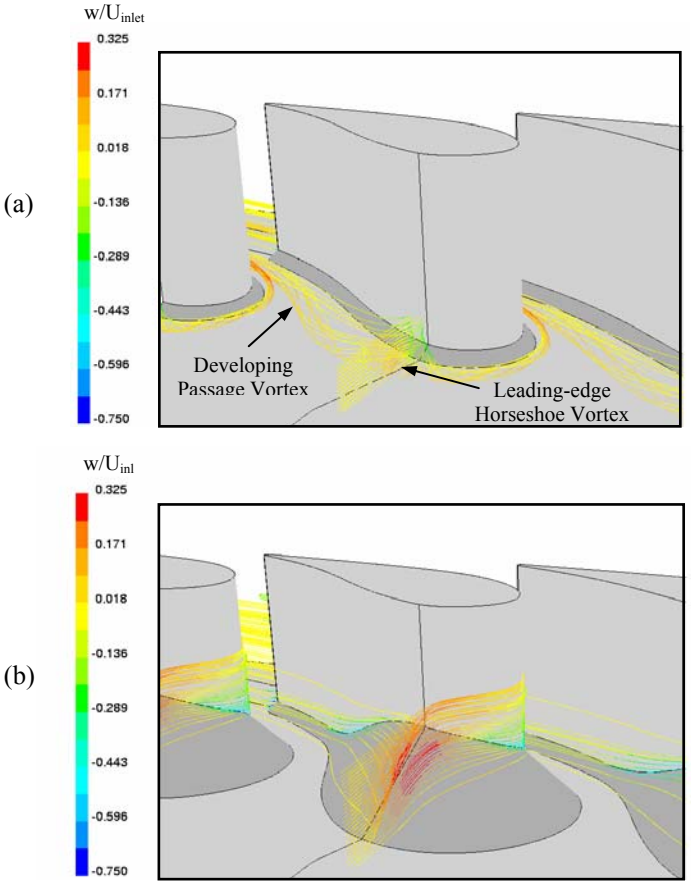

Figure 7a-b. Comparison of streamline patterns for the baseline and optimized filleted vane.

contour of the fillet. While the maximum magnitude of the w-component in the filleted vane is stronger than for the baseline, this maximum occurs as the flow is accelerated up the fillet.

Normalized adiabatic wall temperatures are shown in Figures 8a-b for the baseline and for the optimized filleted vanes. Lower adiabatic wall temperatures for the filleted vane are

indicated in Figures 8b relative to the baseline. These lower temperatures occur not only in the leading edge region but throughout the entire passage.

Table 1 quantifies the actual reduction in the adiabatic wall temperatures for the filleted vane surface. As such, the area-weighted temperatures will be presented in the remainder of this paper. The two quantities given in Table 1 are for the square of the average temperature and one for the maximum temperature. The percent reduction is based on the ratio of the differences of adiabatic wall temperatures for the filleted vane to that of the baseline geometry relative to the total driving temperature potential ($T_{ms} - T_c$) as shown below

$$\%reduction = \frac{\sqrt{\overline{T_{aw}^2}}\Big|_{baseline} - \sqrt{\overline{T_{aw}^2}}\Big|_{fillet}}{T_{ms} - T_c} \qquad (4)$$

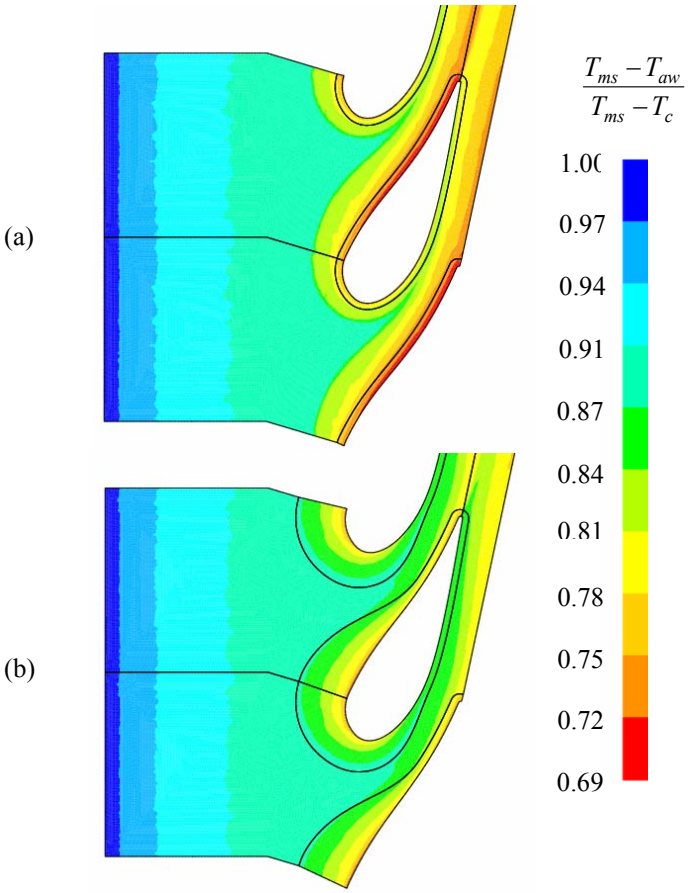

Figure 8a-b. Comparison of adiabatic wall temperatures for the baseline and optimized filleted vane.

where $\sqrt{\overline{T_{aw}^2}}$ is the area-weighted square of the adiabatic wall temperature. The midspan (ms) to coolant (c) driving temperatures remained the same for the filleted and baseline cases. Although the objective function used was the square of the area-weighted temperature, the results between the square of the area-weighted temperatures and the area-weighted temperature were nominally the same. Note that Table 2 indicates each individual surface that was considered. For example, the pressure fillet surface has a 213% increase in area because the comparison is being made between the manufacturing fillet and the optimized fillet that is quite a bit larger. For the filleted vane the total surface area was reduced (including vane, fillet, and endwall) by 2.65% relative to the baseline. Reduced surface area occurs as the fillet becomes larger since the hypotenuse of a triangle is a smaller distance than the combined distances of the sides of a triangle. This reduction in surface area results in less coolant required for the surface area.

Table 2. Summary of Benefit for the Optimized Fillet

Geometric Feature	% Reduction in Temperature (Eq. 4)	% Reduction in Maximum Temperature	% Increase in Surface Area
Fillet Suction Surface	5.1	1.1	205
Fillet Pressure Surface	10.5	4.4	213
Vane Suction Surface	4.1	0	-8.11
Vane Pressure Surface	4.6	0	-12.2
Endwall	3.2	7.5	-37.27
Net Reduction	6.3		-2.65

The component showing the highest reduction in temperature was the fillet along the pressure surface, which was 10.5%. The net thermal benefit considering all of the surfaces was a 6.3% reduction in surface temperatures. The highest peak temperature reduction occurred on the endwall itself, which is particularly important, given the fact that this area is quite hard to cool. In relating these numbers to an engine, consider a main gas path temperature of 1700°C (T_{ms}), a coolant temperature of 600°C (T_c), and a metal temperature of 1250°C (assume to be T_{aw}). If the average adiabatic wall temperature were reduced by 6.3%, it would result in a decrease of metal temperature for the filleted vane by 69°C giving a metal temperature of 1181°C. This reduction in metal temperature would significantly increase component life.

Although Table 1 presents some comparisons between the baseline and filleted vanes, it is difficult to make a one to one comparison since the areas are also changing. For example, consider a large fillet where the vane and endwall surface areas are significantly reduced while the fillet surface areas are significantly increased relative to the baseline geometry. To further assess the improvement, surface-averaged adiabatic wall temperatures as a function of the vane span position were computed for the vane. Note that these averages were computed over a region that extended 5% of the vane span for the entire surface around the vane with the exception of the z/S=0 location in which the endwall surface was averaged. Figure 9 presents these non-dimensional temperatures for the baseline and filleted vanes along with the temperature profile at the inlet to the vane passage. These results indicate that there is not only an affect on the endwall but that there is a thermal benefit along the vane span. The largest difference between the baseline and filleted vanes (peak benefit) occurred at the 20% span location, which is above the maximum height of the fillet.

Flow and Thermal Field Comparisons

Several planes defined perpendicular to the vane, as illustrated in Figure 10, were analyzed for comparisons between the baseline and filleted vane. For all planes except plane SP, coordinate and velocity transformations previously described by Kang and Thole [18] were used to calculate the

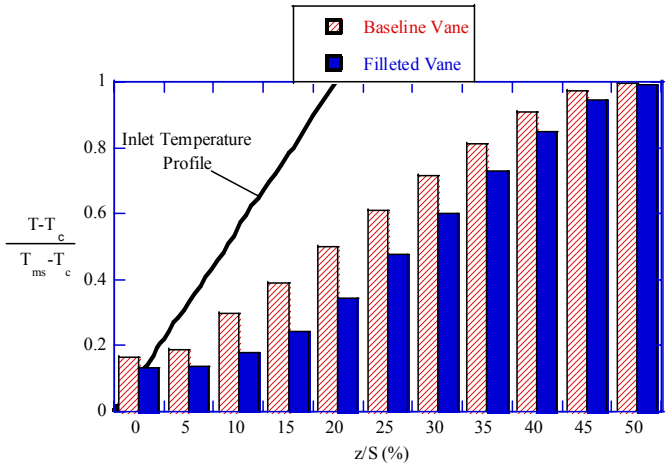

Figure 9. Comparison of area-weighted average adiabatic wall temperatures at each span position for the baseline and optimized filleted vanes.

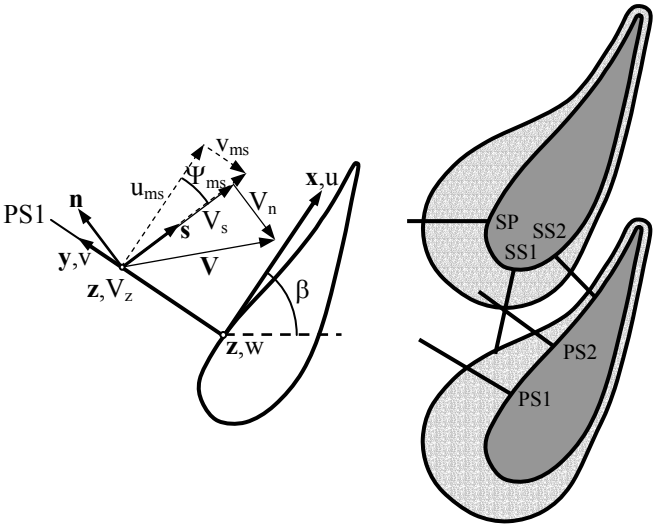

Figure 10. Velocity vector and coordinate transformations for secondary flow analyses.

with the variables defined in the nomenclature of this paper. Since plane SP is oriented parallel to the incoming flow, no transformation was necessary.

The typical leading edge vortex is the result of a spanwise total pressure gradient due to the lower momentum boundary layer flow on the endwall. Higher total pressure away from the endwall drives flow toward the vane-endwall junction resulting in a vortex. Figure 11a-d shows a comparison of the flow results between the baseline geometry of the current secondary flows. That transformation is illustrated in Figure 10 investigation and the best performing fillet in the SP plane. In addition to velocity vectors, contours of temperature are also illustrated to show the influence of the fillet on the approaching thermal field. For the baseline manufacturing fillet case, the velocity vectors clearly show the formation of a horseshoe vortex. Also shown is a distinct flow split on the vane leading edge at approximately 15% span. Above 15% span, the flow is observed to turn upward toward midspan, while below 15% span the flow turns downward toward the endwall. Coincident with this vortex is a distortion of the thermal field with higher temperature fluid being pulled toward the vane-endwall junction. In contrast to this flow situation, the results for the best fillet simulation illustrate the advantages of fillet application. These results show an upturning of the flow along the surface of the fillet and the absence of a leading edge horseshoe vortex. This acceleration of the boundary layer fluid in the spanwise direction enables the flow to overcome the total pressure gradient responsible for horseshoe vortex development. One of the advantages of the fillet design is the resulting thermal field. Unlike the baseline case, the thermal field indicates a positive migration of cooler boundary layer fluid being driven up the fillet. This has the effect of spreading cooler fluid over a larger area of the vane and endwall, and prevents penetration of hotter fluid to these surfaces.Proceeding along the pressure surface of the vane, the flow and thermal field results for the PS2 plane are presented in Figure 12a-d. For the baseline case, growth of the pressure side leg of the horseshoe vortex is apparent, as it begins to develop and merge with cross passage boundary layer fluid to form the

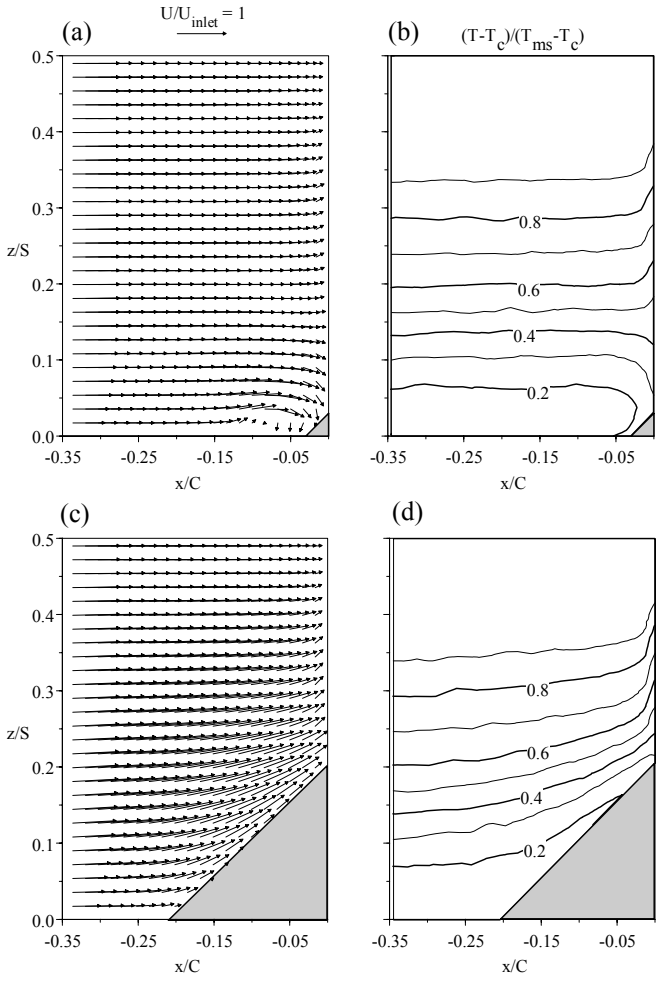

Figure 11a-d. Stagnation flow and thermal contours for the baseline(a,b) and filleted(c,d) vane cases.

passage vortex. Similar to the results in the SP plane, there is significant distortion of the thermal field due to the secondary flows. The results for the best fillet case do not show any definitive vortex structure, however, there are secondary flows that are present. There is a down-turning of the flow below 18% of the span along the pressure side of the vane. Despite this down-turning flow, there is still relatively cool fluid along most of the endwall. In comparison with the baseline case, regions of hotter fluid are significantly skewed toward the vane midspan.

Proceeding from the stagnation plane along the suction surface, the flow and thermal field results for SS2 are given in Figures 13a-d for the baseline and filleted case. The results for the baseline case show the presence of the passage vortex. At this location, any remnants of the suction side leg of the horseshoe vortex have nearly dissipated. The thermal field indicates the accumulation of colder flow toward the suction surface. This accumulation is explained by the strong cross-passage pressure gradient and action of the passage vortex. The results for the filleted vane do not indicate the presence of a passage vortex, however the presence of a strong cross passage flow is clearly evident. Throughout a large portion of the plane a general down-turning of the flow is shown. This is believed to be the result of diminishing fillet size through the passage. As the fillet decreases in height, the streamlines follow the contour of the fillet as shown in Figure 7b. The effect of the strong cross passage flow on the thermal field is also evident in the plot with the migration of colder fluid down the pressure surface and toward the suction surface. Although this distortion is unfavorable, the results for the filleted case still maintain an advantage over the baseline case.

The presence of the fillet results in an improved thermal field, prevents the formation of a leading edge horseshoe vortex, and appears to eliminate full development of a passage vortex. From an aerodynamic perspective, there is a slight increase in the total pressure loss and a deviation of the flow angles. Yaw and pitch flow angles are shown in figures 14a-d for the filleted and unfilleted vanes in the ss2 plane. Note that the yaw angle contours are presented with respect to the flow turning at the vane mid-span.

The results for the baseline case, shown in figures 14a-b, clearly indicate the presence of the passage vortex. The positive values for f, representing the pitch angle, and negative deviation angles for $(y-y_{ms})$, representing the yaw, clearly both indicate the presence of the passage vortex for the baseline

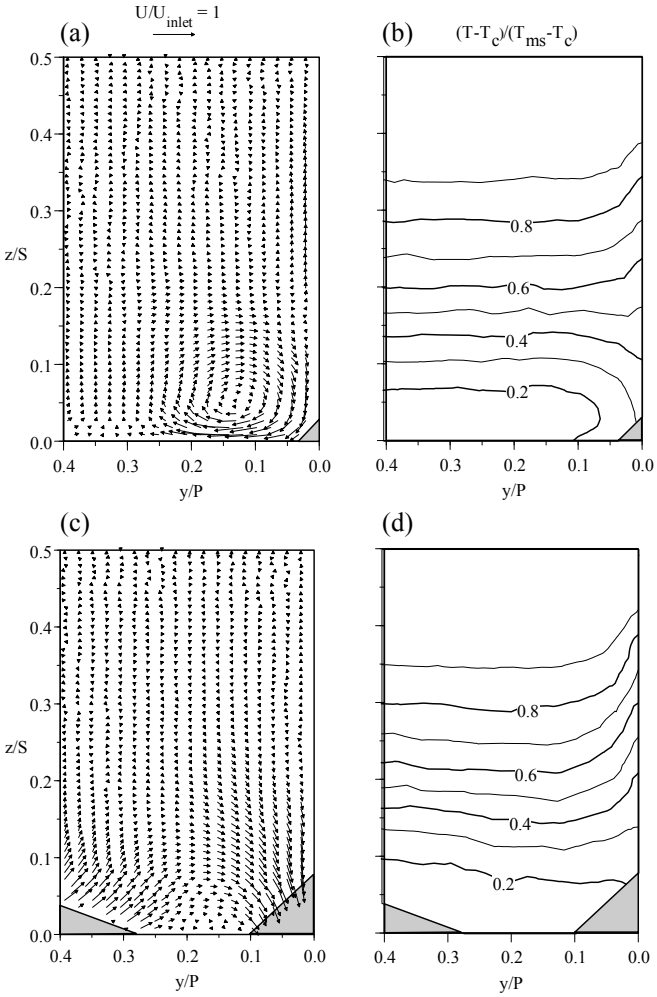

Figure 12a-d. PS2 flow and thermal contours for the baseline (a,b) and filleted(c,d) vane cases.

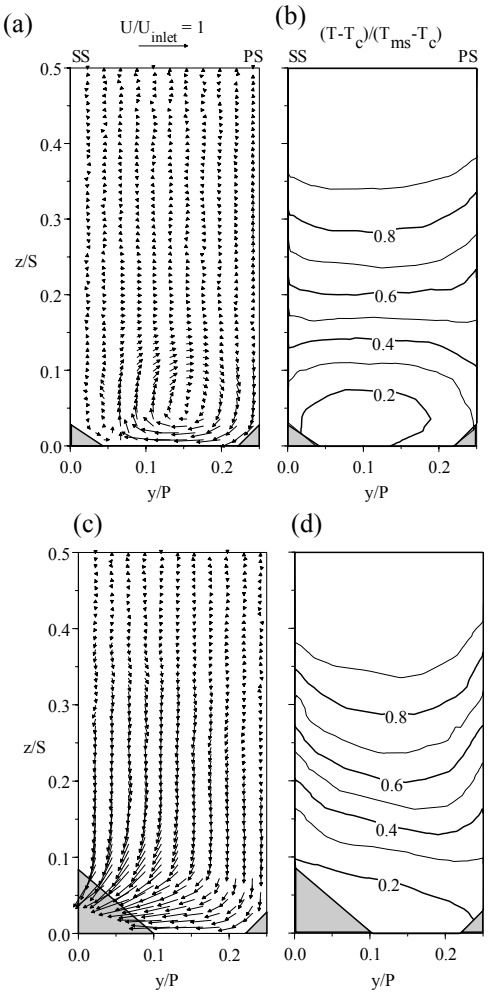

Figure 13a-d. SS2 flow and thermal contours for the baseline (a,b) and filleted(c,d) vane cases.

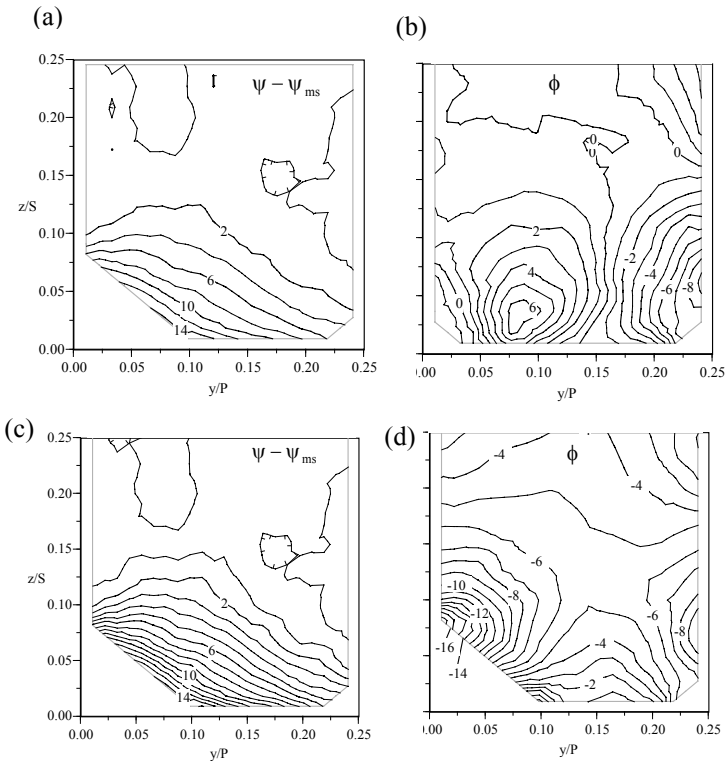

Figures 14a-d Relative yaw and pitch angles in the SS2 planes for baseline (a,b) and filleted (c,d) vanes.

case. With the fillet, negative deviation of ($\psi-\psi_{ms}$) is virtually eliminated in contrast to the baseline case. The larger positive deviation angles for the yaw adjacent to the fillet are due to the flow following the fillet surface. At this location, the fillet is tapering into the suction surface, therefore the near-wall fluid has high positive yaw deviation angles. The filleted case indicates negative values of pitch in the near-wall region as a result of the fillet tapering into the endwall. This flow angles result in a better thermal performance for the combined endwall, vane, and fillet surfaces as was indicated in Figures 13d.

CONCLUSIONS

While several different techniques of secondary flow reduction have been presented in the open literature, to date only the aerodynamic benefits of these techniques have been considered. Based on this study, it is believed that a thermal benefit can also be derived from the use of these techniques, and that these benefits would have an impact on gas turbine development. The objective of this investigation was to optimize the shape of a vane leading edge fillet in order to maximize the thermal benefit of the fillet application. These results demonstrate the merit of using a combined approach of CFD and optimization algorithms.

The optimization results indicated that a large fillet was needed for the maximum thermal benefit and that this benefit was most influenced by the height of the fillet. While a thermal benefit was predicted for the endwall, the maximum predicted benefit occurred on the vane itself at the 20% span location**.** Analysis of the filleted vane indicated that three benefits were realized with a fillet. First, there is a reduction in the overall surface area that needs to be cooled when considering the combined fillet, endwall, and vane surfaces. Second, there is a reduction of the secondary flows resulting from the acceleration of the flow in the endwall region, which prevents the flow from separating and forming a leading edge. Note that this pressure side leg of the leading edge vortex promotes the passage vortex formation. The acceleration caused by the fillet in the leading edge leads to a flat total pressure profile along the vane span. Third, the a reduction of the secondary flows for the filleted vane allows cooler near-wall fluid to remain along the endwall and fillet surfaces rather than being lifted it into the hot mainstream for a case having a strong passage vortex.

ACKNOWLEDGMENTS

The authors would like to acknowledge United Technologies-Pratt & Whitney for their support of this work. We would also like to thank the Air Force Research Laboratory – Turbine Branch and Matt Meininger, in particular, for support of this work.

NOMENCLATURE

C = true chord of turbine vane
C_p = pressure coefficient, $(p_s - p_{s,inlet})/(\frac{1}{2}\rho U_{inlet}^2)$
D_{max} = maximum extent of fillet normal to the vane surface
$F(\mathbf{X})$ = optimization objective function
$F_{norm}(\mathbf{X})$ = normalized optimization objective function using baseline vane results
H_{max} = maximum height of the fillet
n = coordinate normal to inviscid streamline
p_s = static pressure
P = pitch
p_o = total pressure
Re_{in} = turbine cascade inlet Reynolds number, $U_{inlet}C/\nu$
S = span of turbine vane
T = static temperature
u,v,w = local flow plane, transformed velocity components
U,V,W = absolute velocity components
U_{inlet} = vane cascade inlet freestream velocity
V_s = streamwise velocity component, $u\cos\Psi_{ms}+v\sin\Psi_{ms}$
V_n = normal velocity, $-u\sin\Psi_{ms}+v\cos\Psi_{ms}$
V_z = spanwise velocity, w
$\mathbf{X}$ = vector of design variables
x,y,z = local coordinate system
X,Y,Z = global, stationary, coordinate system

Greek

δ = boundary layer thickness
ρ = density
ν = kinematic viscosity
ψ = yaw angle, $\tan^{-1}(v/u)$
ϕ = pitch angle, tan-1(w/u)

Subscripts

aw = adiabatic wall conditions
b = mass-averaged variable
c = coolant conditions
$inlet$ = inlet value at mid-span
ms = midspan values

REFERENCES

[1] Harvey, N.W., Rose, M.G., Taylor, M.D., Shahpar, S., Hartland, J., and Gregory-Smith, D.G., 1999, "Non-Axisymmetric Turbine End Wall Design: Part I Three-Dimensional Linear Design System," ASME 99-GT-337.

[2] Hartland, J.C., Gregory-Smith, D.G., Harvey, N.W., and Rose, M.G., 1999, "Non-Axisymmetric Turbine End Wall Design: Part II Experimental Validation," ASME 99-GT-338.

[3] Gregory-Smith, D. G., Cleak, J. G. E. ,1992, "Secondary Flow Measurements in a Turbine Cascade with High Inlet Turbulence," *ASME J of Turbomachinery*, Vol. 110, pp. 1 - 8.

[4] Brennan, G., Harvey, N.W., Rose, M. G., Fomison, N., Taylor, M., 2001, "Improving the Efficiency of the Trent 500 HP Turbine Using Non-Axisymmetric End Walls: Part 1: Turbine Design," ASME 2001-GT-0444.

[5] Rose, M. G., Harvey, N.W., Seaman, P., Newman, D. A., McManus, D., 2001, "Improving the Efficiency of the TRENT 500 HP Turbine Using Non-Axisymmetric End Walls: Part 2: Experimental Validation," ASME 2001-GT-0505.

[6] Sauer, H., Műller, R., and Vogeler, K., 2000, "Reduction of Secondary Flow Losses in Turbine Cascades by Leading Edge Modifications at the Endwall," ASME 2000-GT-0473.

[7] Zess, G. A. and Thole, K. A., 2002, "Computational Design and Experimental Evaluation of Using a Leading Edge Fillet on a Gas Turbine Vane," *J of Turbomachinery*, vol. 124, pp. 167-175.

[8] Shih, T. I-P. and Lin, Y.-L., 2002, "Controlling Secondary-Flow Structure by Leading-Edge Airfoil Fillet and Inlet Swirl to Reduce Aerodynamic Loss and Surface Heat Transfer," ASME GT-2002-30529.

[9] Fluent Inc., *Fluent User's Guide*, Version 5.0, 1998 (Fluent Inc.: New Hampshire).

[10] Fluent Inc., *Gambit I Modeling Guide*, 1998 (Fluent Inc.: New Hampshire).

[11] Engineous Software, Inc., iSIGHT Designer's Guide, Version 5.0, 1999 (Engineous Software, Inc.: North Carolina)

[12] Yakhot V., Orszag S., Thangman, S., Gatski, T.B., and Speziale, CG., "Development of Turbulence Models for Shear Flows by a Double Expansion Technique," *Phys. Fluids* A 4 (7), 1992, p. 1510.

[13] Kim, S.-E., and Choudhury, D. (1995) "A Near-Wall Treatment Using Wall Functions Sensitized to Pressure Gradient," ASME FED Vol. 217, Separated and Complex Flows.

[14] Radomsky, R., and Thole, K.A., 2000, "Highly Turbulent Flowfield Measurements Around a Stator Vane," *J of Turbomachinery*, Vol. 122, pp. 255-262.

[15] Radomsky, R., and Thole, K.A., 2000, "High Freestream Turbulence Effects in the Endwall Leading Edge Region," *J of Turbomachinery*, Vol. 122, pp. 699-708.

[16] Radomsky, R. R. and Thole, K. A., 2002, "Detailed Boundary Layer Measurements on a Turbine Stator Vane at Elevated Freestream Turbulence Levels," *J of Turbomachinery*, vol. 124, pp. 107-118.

[17] Hermanson, K.S., and Thole, K.A., 2000, "Effect of Inlet Conditions on Endwall Secondary Flows," *J of Propulsion*, Vol. 16, No. 2, pp. 286-296.

[18] Crawford, M.E., 1994, TEXSTAN: A Program for Numerical Computation of Two-Dimensional Internal and External Boundary Layer Flows, Manual TEXSTAN.

[19] Kang, M., and Thole, K.A., 2000, "Flowfield Measurements in the Endwall Region of a Stator Vane," *J of Turbomachinery,* Vol. 122, pp. 458-466.